Contrasts in the 77 K Emission Spectra, Structures, and Dynamics of Metal-to-Metal and Metal-to-Ligand Charge-Transfer Excited States†

Yuan-Jang Chen,‡,§ John F. Endicott,*,‡ and Patrick G. McNamarra‡

Department of Chemistry, Wayne State University, Detroit, Michigan 48202, and Department of Chemistry, Fu Jen Catholic University, Taipei Hsien 24205, Taiwan, Republic of China

Received: December 20, 2006; In Final Form: February 13, 2007

The 77 K emission spectrum of *trans*-[(*ms*-Me_6[14]aneN_4)Cr(CNRu$(NH_3)_5)_2]^{5+}$ has components characteristic of ligand field (LF) and metal-to-metal charge transfer (MMCT) excited states (*ms*-Me_6[14]aneN_4 = 5,12-*meso*-5,7,7,12,14,14-hexamethyl-1,4,8,11-tetraazacyclotetradecane). The LF component of the emission is best resolved for irradiations at appreciably higher energies than the MMCT absorption band, while only the MMCT emission is observed for irradiations on the low-energy side of the MMCT absorption band. The LF emission component from this complex has vibronic structure that is very similar to that of the *trans*-[(*ms*-Me_6[14]aneN_4)Cr$(CN)_2]^+$ parent, but it is red-shifted by 560 cm^{-1} and the bandwidths are much larger. The red shift and the larger bandwidths of the ruthenated complex are attributed to configurational mixing between the LF and MMCT excited states, and the inferred mixing parameters are shown to be consistent with the known electron-transfer properties of the Ru$(NH_3)_5$ moieties. The MMCT excited-state lifetime is about 1 μs at 77 K and am(m)ine perdeuteration of this complex leads to an isotope effect of $k_{NH}/k_{ND} \sim 15-20$. However, the contribution of the N−H stretching vibration to the emission sideband is too weak for a single vibrational mode model to be consistent with the observed lifetimes or the isotope effect. These features are very similar to those reported previously (*J. Phys. Chem. A* **2004**, *108*, 5041) for the MMCT emission of *trans*-[([14]-aneN_4)Cr{CNRu$(NH_3)_5\}_2]^{5+}$ ([14]aneN_4 = 1,4,8,11-tetraazacyclotetradecane), with the exception that the higher energy LF emission was not well resolved in the earlier work. The energies of the charge transfer absorption and emission maxima of both of these Cr(CN)Ru complexes are very similar to those of $[Ru(NH_3)_4bpy]^{2+}$, but the latter has a 50-fold shorter 77 K excited-state lifetime, a 10-fold smaller NH/ND isotope effect, and a very different structure of its vibronic sidebands. Thus, the vibronic sidebands imply that the dominant excited-state distortions are in the metal−ligand vibrational modes for the Cr(CN)Ru complexes and in the bipyridine vibrational modes for the $[Ru(NH_3)_4bpy]^{2+}$ complex. While an "equivalent" single vibrational mode model based on the frequencies and amplitudes of the dominant distortion modes is not consistent the observed lifetimes, such models do appear to be a good basis for qualitatively distinguishing different classes of excited-state dynamic behavior. A multimode, multichannel model may be necessary to adequately describe the excited-state dynamics of these simple electron-transfer systems.

Introduction

During the past several decades there have been appreciable advances in clarifying the relationships between the differences in the molecular structures of the reactants and products with the patterns of electron-transfer reactivity.[1−13] The general principles that have evolved for a semiclassical description of electron-transfer reactivity when the driving force of the electron-transfer step, ΔG^o_{et}, is small in magnitude with respect to the overall nuclear reorganization energy, λ_r, have been used to critically examine a number of very basic issues of reaction mechanisms, provide a systematic basis for predicting the variations in electron-transfer reactivity with reactant structural variations, and facilitating the design of electron-transfer reagents for many different applications.[14] However, the principles governing electron-transfer dynamics when $\Delta G^o_{et} \gg \lambda_r$ (the "Marcus inverted region") are not so well established. It is convenient to represent electron-transfer rate constants in terms of a transition state or semiclassical formalism[7]

$$k_{et} = \kappa_{el}\kappa_{nu}\nu_{nu} \quad (1)$$

where κ_{el} and κ_{nu} are the electronic and nuclear transmission coefficients and ν_{nu} is the vibrational frequency along the critical reaction coordinate. In terms of this formalism, the differences in reactant and product molecular structure contribute to the rate constant through κ_{nu} while issues related to the electronic contributions to reactivity are contained in κ_{el}. The differences in reactant and product (or excited and ground state) structures can be represented in terms of those vibrational normal modes, ν_k, of the lowest energy state which correlate with the differences in molecular structure and for which the squared displacement of the reactant state along the respective nuclear coordinates is represented by a vibrational reorganizational energy, λ_k. The

* To whom correspondence should be addressed. E-mail: jfe@chem.wayne.edu.

† Part of the special issue "Norman Sutin Festschrift".

‡ Wayne State University.

§ Fu Jen Catholic University.

10.1021/jp068781z CCC: $37.00
Published on Web 04/18/2007

structural dependence of k_{el} for a single distortion mode k can then be expressed as[8−10]

$$(\kappa_{nu})_k \approx \sum_j \left[\frac{1}{j!}\left(\frac{\lambda_k}{h\nu_k}\right)^j\right][e^{-\{G_k^2/4RT\lambda_s\}}] \quad (2)$$

$$G_k \approx \Delta G^o_{et} - \lambda_s - jh\nu_{k(max)} \quad (3)$$

where λ_s represents the contributions of solvent or other low-frequency vibrational modes (formally this requires the use of reorganizational free energies rather than energies, but the distinction is ignored here for simplicity). These distortion modes also determine the emission (and to some degree absorption) bandshapes, and the variations of these bandshapes can be useful measures of the variations in excited-state structure.[15−23] Thus, for $|\Delta G^o_{et}|$ sufficiently large relative to $RT\lambda_s$ the lowest energy excited state may emit and the electron-transfer distortion mode contributions to the emission band shape can be represented in a manner that is very closely related to their contributions to electron-transfer rate constants in eq 2, and direct comparisons of excited-state structures and reactivity may be possible. In this paper we compare the contrasting patterns of back electron transfer (or nonradiative decay) of metal-to-metal charge transfer (MMCT) to metal-to-ligand charge transfer (MLCT) excited states of simple transition metal complexes in order to gain further insight into the factors governing inverted region electron transfer.

An important potential application of electron-transfer structure−reactivity relations is in the design of transition metal complex reagents for photoinduced charge separation steps in schemes for the utilization of solar energy[24−28] since the charge transfer (CT) absorptions of these complexes are generally in the visible spectral region and molecular CT excited states form a special class of relatively simple, high-energy electron-transfer systems. When $|\Delta G^o_{et}| \gg \lambda_s$ in such complexes, their excited states may persist long enough to be chemically useful, their relaxation to the ground state corresponds to electron transfer in the Marcus inverted region,[5] and the corresponding rate constants can be treated by general electron transfer formalisms.[4,5,8−10,29−32] However, excited-state molecular structures are more difficult to determine than those of ground electronic states and the relationships between excited-state structures and their patterns of electron-transfer reactivity are correspondingly difficult to document. This is an issue of particular concern for transition metal CT excited states because: (1) there are often several electronic excited states whose energies are not much different from that of the lowest energy state;[33,34] and (2) configurational mixing of these electronic excited states can be large.[19] Such configurational mixing can result in a great deal of structural variation of the lowest energy excited states even in series of transition metal complexes which have the same chromophore and would otherwise have identical excited-state distortions in the diabatic limit.[22,23,35−38]

The $[Ru(NH_3)_4bpy]^{2+}$ and *trans*-$[(L)Cr\{CNRu(NH_3)_5\}_2]^{5+}$ complexes (L = a tetraazamacrocyclic ligand) are particularly interesting examples of contrasting CT excited-state behavior. Their CT emission spectra were only recently reported[39,40] and have been described in detail for the former and for the *trans*-$[([14]aneN_4)Cr\{CNRu(NH_3)_5\}_2]^{5+}$ complex.[35−38] The lowest energy CT excited states of these complexes are approximately 12 000 cm^{-1} above their ground states and both have ambient CT absorption maxima at approximately 500 nm with absorptivities of about 4000 M^{-1} cm^{-1}/Ru.[35,36,41,42] However, the latter

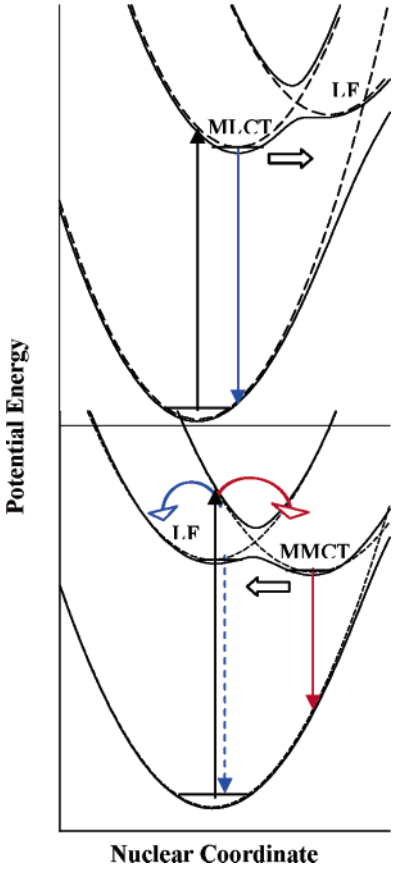

Figure 1. Qualitative PE curves illustrating the general effects of configurational mixing between a ligand field excited state and a lower energy CT excited state in the limits that the lowest energy LF excited state is very distorted (top) and not distorted (bottom). The block arrows indicate the direction of the shift in the nuclear coordinates of the CT PE minima as a result of configurational mixing. The vertical black arrows represent absorption and the vertical red and blue arrows represent emission. The PE minima are arranged for simplicity in the illustration. The red and blue arrows of the bottom panel illustrate the possibility of a dual emission in a Cr(CN)Ru complex.

has about 100 times the 77 K excited-state lifetime of the former and a 5−10 times larger NH/ND kinetic isotope effect,[36,37,40] but the evaluations of its emission spectra and excited-state lifetimes are somewhat complicated by the contributions of a very near in energy ligand field (LF) excited state of Cr(III); this situation is qualitatively represented in Figure 1 (only the two lowest energy electronic excited states are considered for simplicity).

We have now partially resolved the LF emission component in the closely related *trans*-$[(ms\text{-}Me_6[14]aneN_4)Cr\{CNRu(NH_3)_5\}_2]^{5+}$ complex, and this provides an opportunity to

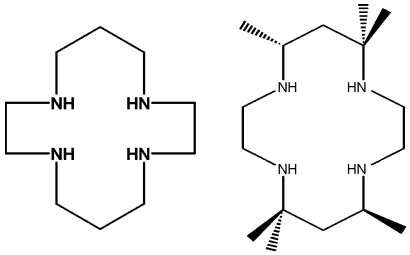

[14]aneN$_4$ **ms-Me$_6$[14]aneN$_4$**

examine the effects of LF/CT excited-state configurational

mixing on CT excited-state behavior. In this report we use emission bandshapes as a basis for distinguishing among types of CT excited-state distortion and as a basis for interpreting the excited-state electron-transfer reactivity in transition metal excited states. For this purpose, we compare the very different dynamic behavior of metal-to-ligand charge transfer (MLCT) and metal-to-metal charge transfer (MMCT) excited states that are nearly identical in energy.

Experimental Section

1. Materials and Synthesis of Compounds. The ligands 2,2-bipyridine (bpy) and ethylenediamine (en) and the metal complex $[Ru(NH_3)_6]Cl_3$ were purchased from Aldrich and Strem. The synthesis and characterization of 1,4,8,11-tetraazacyclotetradecane ([14]aneN$_4$ or cyclam) and 5,12-*meso*-5,7,7,-12,14,14-hexamethyl-1,4,8,11-tetraazacyclotetradecane (Me$_6$-[14]aneN$_4$ or teta) have been described previously.[43−50] The metal complexes $[Ru(NH_3)_5Cl]Cl_2$,[51] *cis*-$[Ru(NH_3)_4Cl_2]Cl$,[51] $[Ru(NH_3)_5(H_2O)](PF_6)_2$,[51] *cis*-$[Ru(NH_3)_4(H_2O)_2](PF_6)_2$, $[Cr([14]\text{-aneN}_4)(CN)_2](PF_6)$,[52] and $[Cr(ms\text{-}[14]\text{aneN}_4)(CN)_2](PF_6)$[53] were synthesized according to literature procedures. Literature syntheses were used for the $[Ru(NH_3)_4bpy](PF_6)_2$ and the *trans*-$[(L)Cr\{CNRu(NH_3)_5\}_2](PF_6)_5$ complexes with L = [14]andN$_4$ and *ms*-Me$_6$[14]aneN$_4$.[35,54−56]

2. Instrumentation. Emission spectra in 77 K glasses were obtained as described in detail elsewhere[35,36] using a calibrated (Xe emission lines for wavelength and an Oriel model 63358 Quartz Tungsten Halogen QTH lamp for intensity) Princeton Instruments (Roper Scientific) OMA V InGaAs array detector (512 pixels) mounted on an Acton SP500 spectrometer with a 300 grooves/mm grating, blazed at 1000 nm. The effective observation window was approximately 150 nm for each setting in the scan−accumulate−paste mode of the WinSpec program. A model 1907-450W xenon lamp with the SPEX model 1680 double-grating spectrometer was used for the 395 and 420 nm irradiations, and the continuous wave 532 nm excitation was provided by MGL-S-B 50 mW 532 nm diode laser modules (Changchun Industries Optoelectronics Tech Co. Ltd.) purchased from OnPoint Lasers, Inc. ASCII files were transferred to EXCEL and up to 30 spectra were averaged for each complex. We used a PRA LN 1000 nitrogen-laser-pumped PRA LN 107 dye laser for sample excitation, and the emitted light was passed through an ISA H-100 monochromator to a Hammamatsu 950 photomultiplier tube (PMT). The PMT was coupled to a LeCroy 9310 digital oscilloscope, and data were analyzed using programs developed by OLIS, Inc. (Jefferson, GA).[57]

Cyclic voltammograms (CVs) were obtained in dry CH_3CN using a three-electrode system consisting of a Ag/AgCl reference electrode, a Pt wire counter electrode, and a Pt disk working electrode with a BAS model 100A electrochemical workstation for measurements. The solutions consisted of the complex dissolved in acetonitrile containing 0.1 mol/L tetrabutylammonium hexafluorophosphate as electrolyte. Ferrocene was dissolved in the sample solutions as an internal reference (0.437 V vs Ag/AgCl) for the cyclic voltammograms.

UV−visible spectra were recorded using a Shimadzu UV-2101PC spectrophotometer. The ^{1}H and ^{13}C NMR spectra were obtained using a Varian 300 Hz instrument.

3. Sample Preparation. The low-temperature emission studies were performed using a 57:43 DMSO/water (v/v) mixture or butyronitrile as the solvent. The DMSO/water mixture gave consistently clear glasses at 77 K. Proteo samples were dissolved in the DMSO/H_2O mixture and loaded into a cylindrical (3 mm i.d.) Suprasil luminescence cell. The cell was then inserted into a spectroscopic Dewar and frozen with liquid nitrogen. Deuteration of the am(m)ine moieties in the complexes was performed in an argon atmosphere in a glovebag. The complexes were first dissolved in 99.9% pure deuterium oxide from Cambridge Isotope Laboratories, Inc. After the solution was mildly agitating for 10 min, an excess of $NaPF_6$ was added. The precipitate was collected after 30 min by vacuum filtration; this process was repeated two times. The deuterated precipitate was then dissolved in D_2O, and a 1.72 mL aliquot of this solution was combined with 2.28 mL of DMSO into a 1 cm quartz absorbance cell using an Oxford Benchmate 1000−5000 μL micropipettor. After mixing, 0.5 mL of this sample was removed and placed into a cylindrical (3 mm i.d.), Suprasil luminescence cell; the remaining sample was used to determine the UV−vis absorption spectrum. Spectroscopic grade DMSO was purchased from Fisher Scientific and used as supplied.

4. Band Shape Analysis. We have based our analysis of the vibronic sideband contributions to the emission spectra on a Gaussian component model that is described in detail elsewhere.[22,23,35,36,38] The emission intensity at a frequency ν_m can be represented as[17,58−60]

$$I_{\nu_m} = \frac{64\pi^4}{3h^3c^3 \ln 10} \frac{\nu_m \eta^3 H_{eg}{}^2 (\Delta\mu_{eg})^2}{(4\pi\lambda_s k_B T)^{1/2}} (FC) \qquad (4)$$

where η is the index of refraction, ν_m is the frequency of the incident radiation, $H_{eg}/h\nu_{eg}\Delta\mu_{eg}$ has been substituted for the transition dipole, M_{eg},[17,60,61] H_{eg} is the electronic matrix element, $\Delta\mu_{eg}$ is the difference of excited-state and ground-state dipole moments, λ_s is the reorganizational energy of the solvent and other displacement modes with frequencies $\nu_s < 4k_BT$, and c is the speed of light. In accord with eq 4, the observed emission intensity was divided by the emission frequency, ν_m, and the Gaussian components that represent the emission fundamentals, $I_{\nu_{m(f)}}$, were obtained by scaling the maximum of the resulting curve to 1.00 in the spectral Excel files and deconvolution of $I_{\nu_{m(f)}}$ was deconvoluted from the emission spectrum using Grams32.

On the basis of Gaussian band shapes and a wave packet model and for the contributions of a single vibrational mode, (FC) can be represented by[17,58,59]

$$(FC) = \sum_j F_{j,k}[e^{-\{4G_j{}^2 \ln 2/\Delta\nu_{1/2}{}^2\}}] \qquad (5)$$

$$F_{j,k} = \frac{S_k{}^j e^{-S_k}}{j!}$$

$$S_k = \lambda_k/h\nu_k \qquad (6)$$

$$G_j = E_{ge}^0{}'0 - \lambda_s - jh\nu_k - h\nu_m \qquad (7)$$

The intensity of the fundamental at a frequency ν_m is then

$$I_{\nu_{m(f)}} \cong I_{max(f)} e^{-\{[h\nu_{max(f)} - h\nu_m]^2/(\Delta\nu_{1/2}{}^2/4\ln 2)\}} \qquad (8)$$

5. The Evaluation of the Vibronic Contributions to the Emission Spectra in Frozen Solution. The vibronic contributions to the emission spectra can be organized into the respective sums of first order, $I_{\nu_{m(0'1)}}$, second order, $I_{\nu_{m(0'2)}}$, third order, $I_{\nu_{m(0'3)}}$, etc., Gaussian component contributions.[22,35] The intensity at a frequency ν_m can be represented as the sum of these components[35]

$$I_{\nu_m} \cong I_{\nu_m(f)} + I_{\nu_m(0'1)} + I_{\nu_m(0'2)} + I_{\nu_m(0'3)} + ... \quad (9)$$

The difference spectrum is constructed from the observed emission spectrum, $I_{\nu_m(expt)}$, as[35]

$$I_{\nu_m(diff;exp)} = I_{\nu_m(expt)} - I_{\nu_m(f)} \quad (10)$$

When *rR* parameters are available, a difference spectrum can also be calculated[35]

$$I_{\nu_m(diff;calc)} \cong I_{\nu_m(0'1)} + I_{\nu_m(0'2)} + I_{\nu_m(0'3)} + ... \quad (11)$$

When the amplitude of the difference spectrum is normalized with respect to that of the fundamental component, the difference spectrum can be interpreted as the convolution of the spectral contributions of the vibronic components (e.g., S_k for the first-order components). This presentation of the vibronic sideband contributions tends to emphasize the contributions of the low-frequency distortion modes. High-frequency vibrational modes are more easily evaluated using a spectral presentation based on empirical reorganizational energy profiles[22,23,36,39] (emreps, Λ_x; see the Appendix for a summary of details) where

$$\Lambda_x = h\nu_x\left(\frac{I_{\nu_m(diff)}}{I_{max(f)}}\right) \quad (12)$$

Where $h\nu_x = 2(h\nu_d) - [(h\nu_d)^2 + (\Delta\nu_{1/2})^2/4 \ln 2]^{1/2}$ involves an approximate correction of $h\nu_d = h[\nu_{max(f)} - \nu_m]$ for the non-Gaussian shapes of the functions that are generated. We use the emrep maxima near to $h\nu_x \sim 1500$ cm^{-1} in much of our analysis of trends in excited-state distortions since this is near to the mostly bpy-centered distortion mode with the largest displacement and the differences in the emreps of isotopomers for $h\nu_x = 2000-3300$ cm^{-1} to evaluate the contributions of C−H and N−H vibrational modes.[35−37]

6. Rate Constant Comparisons. In comparisons of the rate constants for nonradiative excited-state decay, it is sometimes necessary to correct observed excited-state lifetimes for the effects of variations in quantum yields. Thus the radiative quantum yield for $[Ru(bpy)_3]^{2+}$ is reported to be 0.34 at 77 K in ethanol/methanol glasses.[62] Combined with an excited-state lifetime, τ, of 4.5 μs, this leads to radiative and nonradiative lifetimes of 12.5 and 6.7 μs, respectively. The rate constant comparisons in this work are based on orders of magnitude considerations only, and the relatively small corrections that arise from variations in quantum yields are neglected.

Results

A. The CT Absorption Spectra. The CT absorption spectra of $[Ru(NH_3)_4bpy]^{2+}$ and related complexes and of the $[(L)Cr\{CNRu(NH_3)_5\}_2]^{5+}$ complexes have been reported and discussed in detail previously.[19,20,23,42,63] For purposes of this report we have included the ambient absorption spectrum of *trans*-$[(ms\text{-}Me_6[14]aneN_4)Cr\{CNRu(NH_3)_5\}_2]^{5+}$ in Figure 2.

The intense MMCT absorption of this complex is only slightly broadened on the high-energy side with respect to a simple Gaussian band shape as illustrated in Figure 2.[64] The difference spectrum based on this Gaussian function is shown in Figure S1[64] and suggests that there are additional peaks at about 21 100 and 28 100 cm^{-1} with absorptivities of about 3100 and 1700 M^{-1} cm^{-1}, respectively. The weak, higher energy absorption at ~28 000 cm^{-1} is typical for this class of complexes[41,42] and is tentatively assigned as a Cr^{III}-centered ligand field absorption. This compares to the LF absorption maxima of the parent *trans*-$[(ms\text{-}Me_6[14]aneN_4)Cr(CN)_2]^{+}$ complex at 23 400 and 29 600 cm^{-1} (absorptivities of 62 and 66 M^{-1} cm^{-1}, respectively). The greater apparent absorptivity of the ruthenated complex in this (21000−30000 cm^{-1}) spectral region may be a consequence of intensity stealing from the MMCT transition combined with overlapping absorptions of different character.

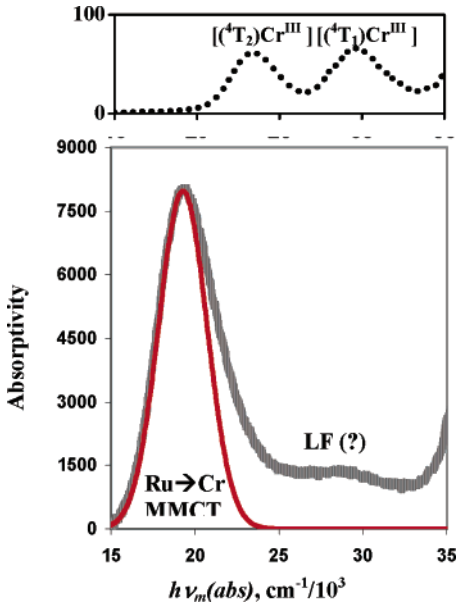

Figure 2. The absorption spectrum of *trans*-$[(ms\text{-}Me_6[14]aneN_4)Cr\{(CNRu(NH_3)_5\}_2]^{5+}$ (thick line) and its single Gaussian component fit (red line). Gaussian peak properties: $h\nu_{max} = 19\,270$ cm^{-1}; $\Delta\nu_{1/2} = 2869$ cm^{-1}. The weak feature designated as LF (?) occurs between 27 000 and 29 500 cm^{-1}. The apparent absorptivity of this feature is ~1700 M^{-1} cm^{-1}. The lowest energy LF absorptions of the *trans*-$[(ms\text{-}Me_6[14]aneN_4)Cr(CN)_2]^{+}$ parent complex are shown in the upper panel (O_h symmetry representations for simplicity to designate the two observed transitions); note that both of these absorptions occur on the high-energy side of the MMCT absorption.

B. The CT Emission Spectra. The CT emission bands of the $[Ru(NH_3)_4bpy]^{2+}$ and $[(L)Cr\{CNRu(NH_3)_5\}_2]^{5+}$ complexes are all relatively weak even at 77 K. The observations on $[Ru(NH_3)_4bpy]^{2+}$ and $[([14]aneN_4)Cr\{CNRu(NH_3)_5\}_2]^{5+}$ are reported elsewhere.[35−38] The MMCT excited-state spectra and lifetimes of the *trans*-$[(L)Cr\{CNRu(NH_3)_5\}_2]^{5+}$ complexes are complicated by the very close in energy (^{2}E)Cr(III) ligand field (LF) excited state,[36,40] while it has been postulated[23,37,38] that configurational mixing of ^{3}MLCT excited state with a close in energy ^{3}LF excited state results in the relatively large displacements in metal−ligand distortion modes observed for $[Ru(NH_3)_4bpy]^{2+}$.[65] Although there has been no direct observation of the ^{3}LF excited state of $[Ru(NH_3)_4bpy]^{2+}$, we have been able to detect contributions from both the (Cr/Ru) MMCT and (Cr^{III}) LF excited states to the emission spectra of *trans*-$[(ms\text{-}Me_6[14]aneN_4)Cr\{CNRu(NH_3)_5\}_2]^{5+}$ in the present study and this has allowed us to address many features of the interactions between the CT and LF excited states.

1. The trans-[(ms-Me$_6$[14]aneN$_4$)Cr{CNRu(NH$_3$)$_5$}$_2$]$^{5+}$ Emission Spectra. The emission spectra of the Cr^{III}-cyano-ruthenates are all complicated by excitation-dependent spectra and lifetimes,[36,40] but this is the only one of these complexes for which we have been able to largely resolve the components of the implicated dual emission that results from the close in energy LF and MMCT excited states.

Irradiations at energies higher than the MMCT absorption clearly show two emission components, one centered at about 12 000 and the other at about 13 500 cm^{-1}, and the higher

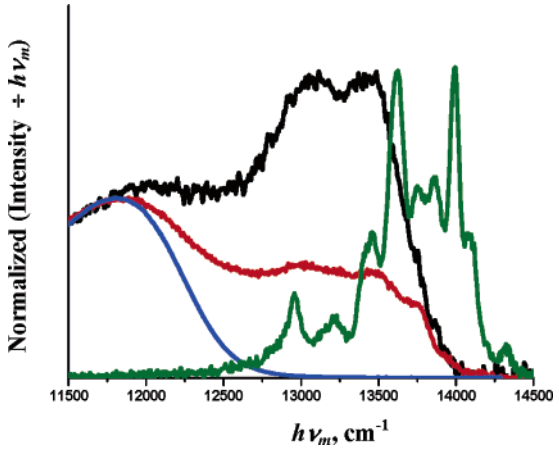

Figure 3. Dual emission components of the *trans*-[(*ms*-Me_6[14]aneN_4)-Cr{CNRu$(NH_3)_5$}$_2$]$^{5+}$ complex (black, red, and blue curves) compared to the emission of the *trans*-[(*ms*-Me_6[14]aneN_4)Cr$(CN)_2$]$^+$ parent (green curve) in 1:1 DMSO/water glasses at 77 K. The black and red curves are the result of 395 nm irradiations of the proteo (NH) and deutereo (ND) isotopomers of the Cr(CN)Ru complex; the blue curve is the result of 532 nm irradiation of *trans*-[(*ms*-Me_6[14]aneN_4)Cr{CNRu$(NH_3)_5$}$_2$]$^{5+}$. The emission spectra have been scaled so that their intensities overlap at about 11 750 cm^{-1}.

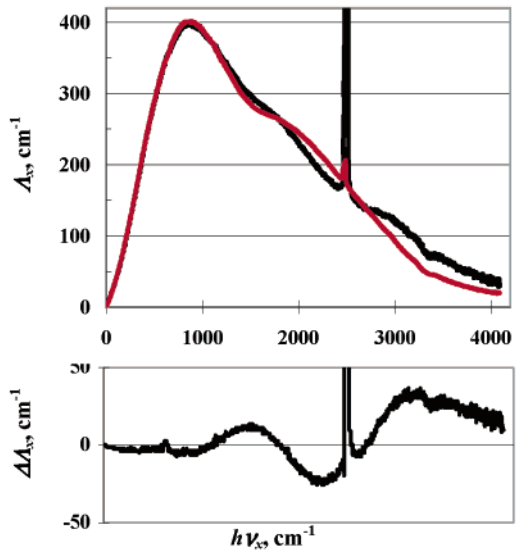

Figure 4. Emreps for NH (black) and ND (red) isotopomers of *trans*-[(*ms*-Me_6[14]aneN_4)Cr{CNRu$NH_3)_5$}$_2$]$^{5+}$ in DMSO/water at 77 K (top). The bottom spectrum is the difference of the isotopomers emreps. The sharp feature at $h\nu_x \sim 2600$ cm^{-1} is from the second-order scattering of the 532 nm excitation in the original emission spectrum.

energy component increases in its percentage contribution as the excitation energy increases (see the black curve in Figure 3). Am(m)ine perdeuteration results in at most a 4-fold increase in the lifetime of the high-energy component, while the lifetime of the low-energy emission component is increased by 15−20 times (Table S1). As a consequence, the lower energy component is much better resolved, even for high-energy irradiations, in the am(m)ine perdeuterated complex (the red curve in Figure 3). Irradiations of the perdeuterated complex on the long wavelength side of its MMCT absorption band result in nicely resolved spectra of the lower energy MMCT emission (the blue curve in Figure 3). We have included the (^{2}E)Cr^{III} emission spectrum of the parent *trans*-[(*ms*-Me_6[14]aneN_4)Cr-$(CN)_2$]$^+$ complex in Figure 3 (green curve) to facilitate direct comparisons in the same medium (1:1 DMSO/water glasses at 77 K) with the higher energy component observed for the 395 nm irradiations of *trans*-[(*ms*-Me_6[14]aneN_4)Cr{CNRu-$(NH_3)_5$}$_2$]$^{5+}$ (black curve). On the basis of the energy differences of the component peaks in the parent LF emission, and assuming that the Stokes and anti-Stokes components have the same energy difference from the 0′0 transition, we assign the weak 14 090 cm^{-1} component in the emission spectrum of the parent *trans*-[(*ms*-Me_6[14]aneN_4)Cr$(CN)_2$]$^+$ complex as the electronic origin of the emission. The high-energy component in the emission of the *trans*-[(*ms*-Me_6[14]aneN_4)Cr{CNRu$(NH_3)_5$}$_2$]$^{5+}$ complex has a pair of broad vibronic components separated by about 400 cm^{-1} (13 450 and 13 040 cm^{-1}; mean $\Delta\nu_{1/2} \approx$ 430 cm^{-1}; based on a Grams32 fit) while the dominant vibronic components of the parent ^{2}E emission are separated by nearly the same energy but appear at about 560 cm^{-1} higher energy (13 991 and 13 618 cm^{-1}; mean $\Delta\nu_{1/2} \approx$ 100 cm^{-1}; based on Grams32 fitting). It should be observed that the likely photochemical impurities, such as *trans*-[(*ms*-Me_6[14]aneN_4)Cr-{CNRu$(NH_3)_5$}(CN)]$^{3+}$, are not centrosymmetric and their emission spectra would be dominated by the band origin (or fundamental component) and the vibronic components would appreciably weaker. Furthermore, the mercuration of the related *trans*-[([15]aneN_4)Cr$(CN)_2$]$^+$ complex results in somewhat broadened emission component bands and an increase in the energy of the 0′0 transition from 13 900 to 14 200 cm^{-1} (see Figure S2);[64] this complex was selected for this purpose because the emission spectra of complexes without an inversion center are dominated by the 0′0 transition.

The comparison of the emreps of the *trans*-[(*ms*-Me_6[14]-aneN_4)Cr{CNRu$(NH_3)_5$}]$^{5+}$, Figure 4, and *trans*-[(*ms*-Me_6[14]-d_4-aneN_4)Cr{CNRu$(ND_3)_5$}]$^{5+}$ [36] isotopomers demonstrates that the N−H stretching modes make small but significant contributions to the emission spectrum.

2. Excited-State Lifetimes of trans-[(ms-Me$_6$[14]aneN$_4$)-Cr{CNRu(NH$_3$)$_5$}$_2$]$^{5+}$. The emissions of this class of complexes are very weak and we were not able to use narrow slits for the H-100 spectrometer attached to the PMT; consequently, all determinations of the excited-state decay rate constants were multiphasic and fitted either to two exponentials (see Table S1)[64] or to the best single exponential (Table 1). The amplitude-weighted mean rate constants obtained from the two exponential fits were about twice as large as those obtained from the single-exponential fits. To the best of our ability to resolve the decay components by adjusting the spectral range of the spectrometer, the higher energy emission component had about 4 times longer lifetime than the low-energy component. The emission decays were also excitation wavelength dependent. The apparent lifetime of the high energy or LF component of the *trans*-[(*ms*-Me_6[14]aneN_4)Cr{CNRu$(NH_3)_5$}$_2$]$^{5+}$ emission is about 10% of that of the Cr(III) parent complex under the same conditions. Am(m)ine perdeuteration increased the longer decay lifetime by 2−6-fold, while perdeuteration of the dicyano parent increased its lifetime 8-fold.[66] The MMCT emission of the *trans*-[(d_4-*ms*-Me_6[14]aneN_4)Cr{CNRu$(ND_3)_5$}$_2$]$^{5+}$ complex has about 15−20 times the lifetime of its proteo (NH) isotopomer (Tables 1 and S1).[64]

C. Attempts To Model MLCT Properties Using Single Mode Models. *1. Fits of the 77 K Emission Spectra.* We have previously noted that single distortion mode approximations generally give poor fits of the 77 K emission band shapes.[22] The discrepancies are most evident in attempts to fit the difference spectra obtained by removing the contributions of the dominant fundamental component from the emission spectrum: $I_{\nu_m(\mathrm{diff})} = I_{\nu_m(\mathrm{obsd})} - I_{\nu_m(\mathrm{f})}$. In principle, the difference spectrum should correspond to the sum of the progressions in the vibrational distortion modes, and this has been demonstrated

TABLE 1: Absorption and Emission Spectral Data and Excited-State Relaxation Rate Constants of Some Cr(III)−CN−Ru(II), Ru(II)−bpy, and Cr(III)−CN Complexes

		77 K emission fundamental				
complexes	absorption υ_{max}, $cm^{-1}/10^3$ [$\epsilon/10^3$][a]	CT emission, $h\upsilon_{max(f)}$ [$\Delta\upsilon_{1/2}$] $cm^{-1}/10^3$ [b,c]	LF emission, $h\upsilon_{max(f)}$ [$\Delta\upsilon_{1/2}$] $cm^{-1}/10^3$	$\Lambda_{h(max)}$ ($h\upsilon_{x'(max)}$), $cm^{-1}/10^3$	$\Delta\Lambda_{h(max)}$ [$h\upsilon_{x'(max)}$][d]	$k_{nr}/(10^6)$, s^{-1} [b,e]
trans-[(*ms*-(5,12)-Me_6[14]aneN_4)Cr-{$CNRu(NH_3)_5\}_2]^{5+}$ [f]	19.2 [8.2] 29.3 [1.9]	11.93 [0.76]	13.45(br) [g]	0.39 (0.81)	 32 [3100]	0.86
trans-[(d_4-*ms*-(5,12)-Me_6[14]aneN_4)Cr-{$CNRu(ND_3)_5\}_2]^{5+}$ [f]		11.91 [0.75]	13.45(br) [g,m]	0.40	−20 [2200]	0.051
trans-[([14]aneN_4)Cr{CNRu-$(NH_3)_5\}_2]^{5+}$ [h]	19.7 [8.0] 28.4 [1.9]	11.99 [0.71]		0.35 (0.83)	 28 [3200]	1.3
trans-[(d_4-[14]aneN_4)Cr{CNRu-$(ND_3)_5\}_2]^{5+}$ [h]		11.98 [0.72]		0.37 (0.83)	−30 [2500]	0.094
$[Ru(NH_3)_4bpy]^{2+}$ [i,j]	18.9 (d/w) 19.0 [4.0] (bun)	12.09 [1.11] (d/w) 12.42 [0.92] (bun)		0.81 (1.45) (d/w) 0.80 (1.48) (bun)	 10 [3300]	39 (d/w) 22 (bun)
$[Ru(ND_3)_4bpy]^{2+}$ [i,j]	18.9 (d/w) 19.2 (bun)	12.10 [1.13] (d/w) 12.41 [0.93] (bun)		0.80 (1.46) (d/w) 0.79 (1.51) (bun)	−10 [2300]	13 (d/w) 12 (bun)
trans-[Cr(*ms*-(5,12)-Me_6[14]ane-$N_4)(CN)_2]^{+}$ [f,k,l]	29.6 [0.062] 23.4 [0.066]		13.99 (d/w)			0.0026
trans-[$Cr(d_4$-*ms*-(5,12)-Me_6[14]ane-$N_4)(CN)_2]^{+}$ [f,k,l]			14.00 (d/w)[m]			0.00033
trans-[Cr([14]aneN_4)$(CN)_2]^{+}$ [f,k,l]	30.1 [0.068] 24.1 [0.063]		13.93 (d/w)			0.0028
trans-[$Cr(d_4$-[14]aneN_4)$(CN)_2]^{+}$ [f,k,l]			13.94 (d/w) [m]			0.00033

[a] 298 K, Cr−CN−Ru and Cr−CN complexes in water, Ru−bpy complexes in DMSO/water (D_2O) (d/w) and butyronitrile (bun). [b] 77 K, Cr−CN−Ru and Cr−CN complexes in DMSO/water (H_2O or D_2O) glasses, Ru−bpy complexes in DMSO/water (H_2O or D_2O) (d/w) and butyronitrile (bun) glasses. [c] Excitation energy, 532 nm, MGL-S−B-50 mW diol laser modules (Changchun Industries Optoelectronics Tech Co. Ltd). [d] $\Delta\Lambda_h = \Lambda_{h(NH)} - \Lambda_{h(ND)}$. [e] Emission fundamental. [f] This work. [g] Excitational energy, 420 nm, by xenon lamp with the model 1680 SPEX double-grating Spectramate; see experiment. [h] Reference 36. [i] Reference 37. [j] Reference 35. [k] Reference 53. [l] Lessard, R. B. Ph. D. Dissertation, Wayne State University, 1988. [m] DMSO/D_2O.

to be the case for the spectra of $[Ru(bpy)_3]^{2+}$ and $[Ru(NH_3)_4$-$bpy]^{2+}$ [35] by using the distortion modes found in their resonance-Raman spectra.[65,67] For single mode fits, we have constructed a "best Gaussian fit" to the highest intensity feature of the difference spectra in Figure S3[64] to represent the best single mode approximation. There are significant contributions to the difference spectra of these complexes in the low-frequency range, $h\nu_d = h\nu_{max(f)} - h\nu_{m(obsd)} < 900\ cm^{-1}$. These contributions apparently arise from significant distortions in the Ru−ligand skeletal modes,[23,35,65,67] and they are partially resolved when the component bandwidths are relatively small as in butyronitrile glasses at 77 K; see Figures S3 and S4.[64] The composite amplitudes of these low-frequency contributions are smaller than those of the bpy skeletal modes ($h\nu_d \sim 1300-1500\ cm^{-1}$) and must be ignored in any attempt to represent the spectrum by a single distortion mode. In addition to this problem, the representation of the difference spectrum in terms of a single distortion mode fitted to the dominant feature of the difference spectrum results in higher order intensity contributions from the vibronic progression in this mode that exceed the observed emission intensities for $h\nu_d > 2000\ cm^{-1}$. As the component bandwidth increases, these problems with the single mode fits decrease in significance even at 77 K (see the fit to the difference spectrum of $[Ru(NH_3)_4bpy]^{2+}$ in DMSO/water glass in the lower right panel of Figure S3).[64] The component bandwidths are typically about twice as large for ambient solutions as for 77 K glasses,[35] and good single mode fits of the resulting structureless emission bands are likely since properties dependent on the collective displacement in a very large number of nuclear coordinates are theoretically expected to be well represented by a reduced number of nuclear coordinates in large molecules.[68] However, these single mode fits of the spectra do not properly represent the structural differences between the ground and excited states in these molecules, they obscure the changes in structure that result from differences in configurational mixing among the electronic states and the low-temperature spectra require more than one mode for reasonable fits both as a matter of principle[68] and in practice. Consequently single mode fits are used only in a limited, qualitative way in the discussions of excited-state structure−reactivity relationships in this study.

2. MLCT Excited-State Nonradiative Relaxation Rate Constant Correlations. In the limit that a single distortion mode contributes to the excited-state relaxation rate constant and for weak electronic coupling limit (H_{eg} small) the decay rate constant may be formulated as[7−10,17,30]

$$(k_{et})_k \approx \frac{2\pi^2}{h}\frac{{H_{eg}}^2}{(\pi\lambda_s k_B T)^{1/2}}\sum_j\left[\frac{1}{j!}\left(\frac{\lambda_k}{h\nu_k}\right)^j\right][e^{-\{G_k^2/4RT\lambda_s\}}] \quad (13)$$

Meyer and co-workers have used single distortion mode expressions related to eq 13 to fit the ambient spectra and lifetimes of several series of tris-polypyridyl complexes of Ru and Os.[69−73] Since the progressions in a single distortion mode do not properly represent the excited-state distortion at 77 K (see Figure S3) a single mode expression is not expected to be quantitatively useful for the excited-state relaxation processes. Apparently the single mode approximation works reasonably well in representing ambient excited-state decay rate constants for these complexes because the multimode dependencies of complex systems can be adequately represented by a single distortion mode for some purposes.[68]

We have examined these issues using an extended range of complexes. If the multimode problem is to be treated in terms of a single distortion mode, then the maximum of the reorganizational energy profile, $\Lambda_{x(max)}$, is a reasonable approximation for the reorganizational energy for such a mode of Ru−bpy complexes, especially since this maximum occurs near to the frequency of the bpy skeletal mode with the largest distortion.[35] We will generalize this and assume that this is always the best

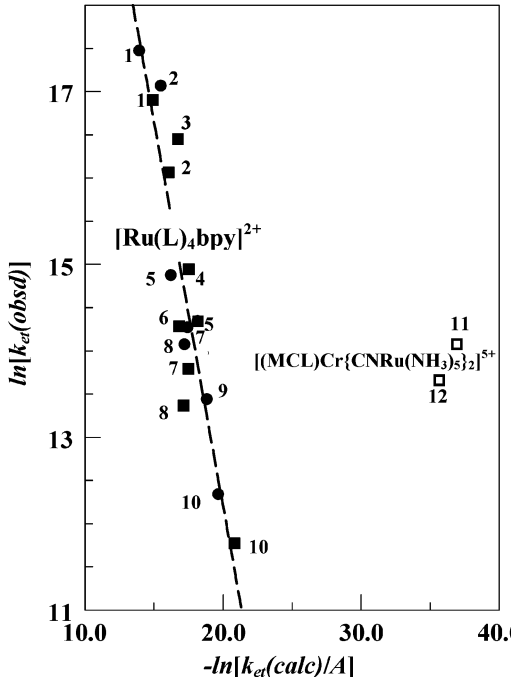

Figure 5. Comparison of the 77 K rate constants observed for CT excited-state decay, k_{et}(obsd), to k_{et}(calc)/A based on eq 14. For $[Ru(L)_4bpy]^{2+}$ complexes, closed circles for DMSO/water solutions and closed squares for butyronitrile solutions. Open squares for *trans*-$[(MCL)Cr\{CNRu(NH_3)_5\}_2]^{5+}$ complexes in DMSO/water glasses. Data from Table 1 and refs 35 and 38 $(L)_4 = (NH_3)_4$, 1; $(en)_2$, 2; trien, 3; [15]aneN$_4$, 4; $(NH_3)_2$bpy, 5; pyo[14]aneN$_4$, 6; [14]aneN$_4$, 7; (en)bpy, 8; *rac*-Me$_6$[14]aneN$_4$, 9; $(bpy)_2$, 10. MCL = [14]aneN$_4$, 11; *ms*-Me$_6$-[14]aneN$_4$, 12.

approximation for the contributions of a single "equivalent" distortion mode. Then the nonradiative rate constant for this single mode limit can be written

$$k_{et}(\text{calcd}) \approx A \sum_j \left[\frac{1}{j!}\left(\frac{\Lambda_{x(\max)}}{h\nu_{x(\max)}}\right)^j\right][e^{-\{G^2/4RT\lambda_s\}}] \quad (14)$$

$$G_k \approx h\nu_{\max(f)} - \lambda_s - jh\nu_{x(\max)} \quad (15)$$

Equation 14 seems to provide a reasonable overall representation of the behavior of the rate constants found for MLCT excited-state decay of the class of $[Ru(Am)_{6-2n}(bpy)_n]^{2+}$ complexes in butyronitrile solutions at 77 K[35,38] (assuming $\lambda_s = 1000$ cm^{-1} for purposes of this comparison) since the slope of the log/log plot of the observed decay rate constant vs the right-hand side of eq 14 is 0.9 ± 0.2 and $A = 10^{13\pm1.7}$ s^{-1} as shown in Figure 5 (the correlation in this figure omits data for the $[Ru(py)_4bpy]^{2+}$, $[Ru([12]aneN_4)bpy]^{2+}$, and $[Ru([12]aneN_4)$-$bpy]^{2+}$ complexes that are known to deviate significantly).[38]

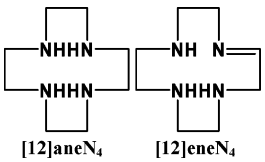

The scatter in this correlation is considerable ($r^2 = 0.76$) and the prefactor A is in the range expected for an adiabatic surface crossing (i.e., for $\kappa_{el} = 1$). The data obtained in DMSO/water for the $[Ru(Am)_{6-2n}(bpy)_n]^{2+}$ complexes with Am = NH_3 or en/2 correlate a little better, as we noted previously,[35] (slope = 0.86 ± 0.07; intercept = 29.3 ± 1.3; $r^2 = 0.94$). However, the observations for the *trans*-$[(MCL)Cr\{CNRu(NH_3)_5\}_2]^{5+}$ complexes deviate dramatically from the correlation line for the Ru−bpy complexes, a deviation that is far greater than that of the other three complexes mentioned above.

Most of the solvent modes are expected to be frozen at 77 K[29] so that $\lambda_s \ll 1000$ cm^{-1} (as employed in the above correlation). Under these conditions the exponential factor in eqs 13 and 14 behaves as a delta function (note that at 77 K, $k_BT = 53$ cm^{-1}) centered on the collections of coupled ground state vibrational modes. For $h\nu_k \ll E^{0'0}$ and very small displacements eq 14 can be put into the form[8,9,37]

$$k_{et} = Ae^{-\gamma_x(h\nu_{\max(f)})/(h\nu_{x(\max)})}, \qquad \gamma_x = \ln(h\nu_{\max(f)}/\Lambda_{x(\max)}) - 1 \quad (16)$$

Correlations based on eq 16 are not significantly different from those discussed above.

Finally, in a single mode system the maximum amplitude of the difference spectrum, normalized so that $I_{\max(f)} = 1.00$, is equal to the Huang−Rhys parameter for the first-order component for this vibrational mode and we have used such single mode fits to the normalized difference spectra as a basis for the parameters in eqs 14 and 16 for the $[Ru(bpy)_3]^{2+}$ and $[Ru(NH_3)_4bpy]^{2+}$ complexes, but the fit of these parameters to the observed rate constants appears to be worse than the emrep parameters since the smaller frequencies of the single mode maxima require larger values of j. It is important to note that (a) the maxima of the difference spectrum and the emrep should occur at the same vibrational frequency for a single mode system,[22] but these maxima differ in their vibrational frequencies in a multimode system when there is overlap of the vibronic contributions, and (b) the vibronic components found in resonance-Raman spectra[65,67] adequately account for the difference spectra and emreps of these complexes.[35]

Despite the reservations noted, it seems that eqs 14 and 16 may provide useful means for qualitatively categorizing different classes of inverted region electron transfer (or excited-state relaxation) behavior,[38,74] even though the parameters obtained from these correlations do not currently have obvious physical significance.

Discussion

We have examined the excited-state behavior of the *trans*-$[(ms\text{-}Me_6[14]aneN_4)Cr\{CNRu(NH_3)_5\}_2]^{5+}$ complex in order to better characterize the properties of the MMCT excited states in Cr(CN)Ru complexes and to gain insight into contrasting excited-state dynamic behavior reported for these and for the MLCT excited state of $[Ru(NH_3)_4bpy]^{2+}$.[35,36] Thus, the energy of this MLCT excited state is nearly identical to the MMCT excited-state energies of the *trans*-$[(MCL)Cr\{CNRu(NH_3)_5\}_2]^{5+}$ complexes (MCL =[14]aneN$_4$ and *ms*-Me$_6$[14]aneN$_4$), but its lifetime is much shorter and its NH/ND isotope effect is much smaller. We recently postulated that configurational mixing with ligand field excited states was a source of some of the larger variations in MLCT excited-state properties found for the $[Ru(Am)_4bpy]^{2+}$ complexes,[38] but experimental information about excited-state/excited-state configurational mixing is very difficult to obtain. The *trans*-$[(ms\text{-}Me_6[14]aneN_4)Cr\{CNRu(NH_3)_5\}_2]^{5+}$ complex is unique in that its emission spectra reveal critical information about the mixing of LF and CT excited states. This and the vibronic sideband contributions to the emission spectra provide useful insights into the contrasts in the CT excited-state behavior of these complexes.

A. The *trans*-[(*ms*-Me$_6$[14]aneN$_4$)Cr{CNRu(NH$_3$)$_5$}$_2$]$^{5+}$ Emission Spectra. *1. Dual LF and MMCT Excited-State Emission.* The emissions in this class of complexes are unique in several ways. For the complexes examined so far:[36,40] (1) the fundamental components of the MMCT emission and of the ^2E emission of the parent dicyano complexes differ by less than 2000 cm^{-1}; (2) the behavior is reproducible, does not change significantly on purification, and is found to varying degrees in each of the complexes of this class; (3) the excited-state lifetimes of all components, for all complexes of this class at 77 K, are more than an order of magnitude shorter than those of the parent cyano−Cr(III) complexes. The *trans*-[(*ms*-Me$_6$-[14]aneN$_4$)Cr{CNRu(NH$_3$)$_5$}$_2$]$^{5+}$ complex is unique among the complexes examined in that it has been possible to largely resolve the emissions of both excited states. Thus, the dominant vibronic components of the high-energy emission spectral band of the *trans*-[(*ms*-Me$_6$[14]aneN$_4$)Cr{CNRu(NH$_3$)$_5$}$_2$]$^{5+}$ complex are very similar to those of the parent *trans*-[(*ms*-Me$_6$[14]aneN$_4$)-Cr{CN}$_2$]$^+$ complex but shifted to significantly lower energy, and this shift to lower energy is unusual for a Cr^{III} complex.

Genuine dual emissions are very rare, and the observation of more than one emission is usually symptomatic of sample impurity. In evaluating the high-energy emission band found for the *trans*-[(*ms*-Me$_6$[14]aneN$_4$)Cr{CNRu(NH$_3$)$_5$}$_2$]$^{5+}$ complex, it is important to keep in mind several characteristic features of the (^{2}E)Cr^{III} emission spectra: (a) the ^{2}E emission energy of monometallic Cr^{III} complexes shifts to lower energy as the number of π-acceptor ligands increases, and the cyano complexes have among the lowest energy ^{2}E emissions;[66,75] (b) the fundamental {e,0′} → {g,0} component is electronically forbidden in centrosymmetric complexes and some or many of the vibronic components of the spectra of such complexes are much more intense than the fundamental component; and (c) the emission spectra of Cr^{III} complexes that lack a center of symmetry are dominated by the fundamental component and the vibronic side bands are relatively weak. Thus, the relatively narrow bandwidths and the dominant vibronic structure of the high-energy emission band of *trans*-[(*ms*-Me$_6$[14]aneN$_4$)Cr-{CNRu(NH$_3$)$_5$}$_2$]$^{5+}$ are qualitatively similar to features in the higher energy emission of the dicyano−Cr(III) parent, and these features indicate that this emission is from a centrosymmetric complex related to, but different from, the dicyano parent. Furthermore, the lifetime associated with the high-energy emission band is less than about10% that of the parent dicyano complex, and like the parent it has a relatively small isotope effect; thus, $k_{NH}/k_{ND} \approx 8$ for the parent and between about 2 (based in Table S1) and 6 (based in Figure 4) for the high-energy band in the ruthenate. Thus, there are no acceptable alternatives to the assignment of the higher energy spectral emission band to the (^{2}E)Cr(III) excited-state of the *trans*-[(*ms*-Me$_6$[14]aneN$_4$)Cr{CNRu(NH$_3$)$_5$}$_2$]$^{5+}$ complex, while the much broader lower energy emission is readily assigned to the Cr/Ru MMCT excited state.

2. Important Features of the trans-[(ms-Me$_6$[14]aneN$_4$)Cr-{CNRu(NH$_3$)$_5$}$_2$]$^{5+}$ Emission Spectrum. a. LF Excited-State MMCT Excited-State Configurational Mixing and Its Implications. We have observed that the ^{2}E emission of a [(L)Cr^{III}-(CNHg)]$^{n+}$ cyano-metalate with a poor electron donor (Hg^{2+}) results in about a 180 cm^{-1} increase of the energy of the ^{2}E emission (Figure S2). Therefore, the 560 cm^{-1} lower ^{2}E emission energy in the *trans*-[(*ms*-Me$_6$[14]aneN$_4$)Cr{CNRu-(NH$_3$)$_5$}$_2$]$^{5+}$ complex than in the dicyano parent suggests that configurational mixing with the MMCT excited state of the ruthenated complex lowers the energy of its ^{2}E excited state by about 600−700 cm^{-1}. This is consistent with the 330 cm^{-1} larger bandwidths of the vibronic components of the LF part of the *trans*-[(*ms*-Me$_6$[14]aneN$_4$)Cr{CNRu(NH$_3$)$_5$}$_2$]$^{5+}$ emission. If we assume $\lambda^o_{LF} = 0$ for the intrinsic reorganizational energy of the ^{2}E excited state with respect to the ^{4}A ground state, then the appreciable component bandwidths of the *trans*-[(*ms*-Me$_6$-[14]aneN$_4$)Cr{CN}$_2$]$^+$ parent are a result of a combination of the limits of instrumental resolution, the overlap of unresolved vibronic components, the small effects of solvational differences, etc., and can be represented as $\Delta\nu_{1/2}(LF)_p \approx \sigma_p$. Configurational mixing between the (^{2}E)Cr^{III} and the two MMCT excited states of *trans*-[(*ms*-Me$_6$[14]aneN$_4$)Cr{CNRu(NH$_3$)$_5$}$_2$]$^{5+}$ will add a component to the bandwidth that most simply can be represented as

$$\Delta\nu_{1/2}(LF) \approx \sigma_p + 2\,\alpha_{CT,LF}{}^2\Delta\nu_{1/2}(CT_{Ru}) \qquad (17)$$

The large bandwidth of the MMCT excited state can arise from some combination of (a) the distribution of different solvent environments of the complexes in the frozen solutions (σ_{CT}) and/or (b) a contribution of $\sim 4(\lambda_i k_B T \ln 2)^{1/2}$ arising from distortion modes with low vibrational frequencies ($h\nu_i < 4k_BT$) which are important when the nuclear coordinates of the ground and excited states are different (note that most of the solvent modes, λ_s, are frozen at 77 K).[29] The second right-hand side term in eq 17 is not entirely appropriate if the emitting MMCT excited state is localized, as seems likely, while the MMCT excited states accessed by ground state light absorption complex are degenerate. However unsymmetrical solvation of the Ru^{II}-(NH$_3$)$_5$ moieties in the frozen solutions will result in slightly different configurational mixings of the nominally degenerate MMCT states with the ^{2}E state analogous to the effect of the distribution of solvent environments on the MMCT emission bandwidths. Thus, the increased bandwidth of the ^{2}E emission in the Cr(CN)Ru complexes and eq 17 suggest that $\alpha^2_{CT,LF} \leq 0.2$. Another consequence of this excited state−excited state configurational mixing is a shift of the MMCT excited-state PE minimum with respect to that of the ground state and the diabatic (^{2}E)Cr^{III} excited state (which has essentially the same nuclear coordinates as the ground state), and a corresponding attenuation of the vibronic sidebands of the MMCT emission since[19,76−78]

$$\lambda_{CT} \approx \lambda^o_{CT}(1 - 2\alpha_{CT,LF}{}^2) \qquad (18)$$

This attenuation can be expressed in terms of the emrep maximum as[35]

$$\Lambda_{x(max;obsd)} \approx \Lambda^o_{x(max;CT)}(1 - 2\alpha_{CT,LF}{}^2) \approx 400\ \text{cm}^{-1} \qquad (19)$$

Thus for $\alpha^2_{CT,LF} \leq 0.2$ (as inferred from the bandwidth), $\Lambda^o_{x(max;CT)} \leq 670$ cm^{-1} and the configurational mixing of the (^{2}E)Cr^{III} and MMCT excited states may significantly reduce the distortion that would otherwise be characteristic of the MMCT excited state.

These parameters can be used to set limits for the values of several excited-state electron-transfer parameters and thereby to ascertain whether the interpretation offered here is consistent with the known properties of these systems. The stabilization of the (^{2}E)Cr^{III} excited-state that arises from its configurational mixing with the two MMCT excited states is apparently $2\,\alpha^2_{CT,LF}E^o_{LF,CT} \approx 700$ cm^{-1} and for $\alpha^2_{CT,LF} \sim 0.2$ the vertical

energy is $E^{o}_{LF,CT} \approx 1750\ cm^{-1}$ and a matrix element $H_{CT,LF} \approx 780\ cm^{-1}$ for the ^{2}E/MMCT "mixed valence" electron-transfer process. For these parameters, the barrier for electron transfer between the degenerate MMCT excited states in the diabatic limit is about $\lambda_r/4 = [E^{o}_{LF,CT} + E^{0'0''}_{LF,CT}] \sim 3200\ cm^{-1}$ (where $E^{0'0''}_{LF,CT}$ is the difference in energy between the vibrationally equilibrated excited states) for $Ru^{II}(NH_3)_5/Ru^{III}(NH_3)_5$ electron transfer between the MMCT excited states of the complex. The value of $\lambda_r \approx 12\,800\ cm^{-1}$ based on the above rough estimates compares well with the value of $\lambda_r \approx 13\,000\ cm^{-1}$ estimated for mixed valence $Ru^{II}(NH_3)_5/Ru^{III}(NH_3)_5$ electron transfer in the ground states of these complexes[21,63,79] and for $[Ru(NH_3)_6]^{2+,3+}$ bimolecular electron transfer[21] in ambient aqueous solutions. Thus, it appears that the overall interpretation is consistent and that the parameters are plausible estimates. However, as illustrated in Figures 1 and S5,[64] the configurational mixing between the ^{2}E/MMCT excited states will result in a smaller barrier for adiabatic electron transfer ($\sim$1500 cm^{-1}, based on reasoning illustrated in Figure S5). These estimates indicate that the (^{2}E)Cr^{III}-mediated superexchange electronic matrix element of $H_{CT,CT'} < 50\ cm^{-1}$ so that the barrier to excited state $Ru^{II}(NH_3)_5/Ru^{III}(NH_3)_5$ electron transfer is $\geq 30k_BT$, consistent with emission from a largely localized ^{2}MMCT excited state.

The appreciable vibronic sideband contributions to the MMCT emission spectra implicate distortion in some vibrational modes for which $h\nu_h > 4k_BT$ and $\Lambda^{o}_{x(max)} \approx 670\ cm^{-1}$ and this would add to the electron-transfer barriers estimated above.

We emphasize that the uncertainties are very large (probably $>$20% and $\leq$50%) in each of the estimates, and they are used here only to illustrate that the spectral assignments are consistent with the information currently available.

B. The Contrasts in MMCT and MLCT Excited-State Properties. The contrasts in lifetimes and in isotope effects are interrelated, but it is convenient to initially consider them separately.

1. The CT Excited States. The absorption and emission energies of the *trans*-$[(L)Cr\{CNRu(NH_3)_5\}_2]^{5+}$ and $[Ru(NH_3)_4bpy]^{2+}$ complexes are very similar (Table 1 and Figure S6), with pseudo-Stokes shifts, $E_{ss} = [h\nu_{max}(abs;300\ K) - h\nu_{max(f)}(emis;77\ K)] \sim 7000\ cm^{-1}$. The contributions to $h\nu_{max}(abs)$ can be attributed to (a) the energy difference between the diabatic PE minima of the ground and CT excited electronic states of the same spin multiplicity, $E_s^{00'}$, (b) the reorganizational energy required to change the nuclear coordinates of the excited state PE minimum to those of the ground state, λ_r, (c) the difference in energy of the HOMO and the orbital that has the largest transition dipole, δ_{orb}, (d) the energy difference that results from configurational mixing between the electronic states, $2\epsilon_s = 2H^2_{ge}/E_s^{00'}$, and (e) a contribution that arises from the convolution of low-frequency vibronic components with the fundamental in broad band spectra, δ_{vib}. Thus

$$h\nu_{max(abs)} \cong E_s^{00'} + \lambda_r + 2\epsilon_s + \delta_{orb} + \delta_{vib} \qquad (20)$$

The contributions to $h\nu_{max(f)}$, obtained by deconvolution of the observed 77 K emission spectrum, can similarly be attributed to (a) the energy difference between the diabatic PE minima of the CT excited and ground electronic states of different spin multiplicities, which can be expressed as $E_s^{00'} - 2K_{exch}$ for a triplet excited-state and a singlet ground state, (b) the energy difference that results from configurational mixing between these electronic states, $2\epsilon_s' = H^2_{eg}/(E_s^{00'} - 2K_{exch})$, and (c) a contribution that arises from the convolution of low-frequency vibronic components with the fundamental in broad bandspectra, δ_{vib}'. Thus, for triplet excited state and a singlet ground state

$$h\nu_{max(f)} \cong E_s^{00'} - 2K_{exch} + 2\epsilon_s' - \delta_{vib}' \qquad (21)$$

Therefore

$$E_{ss} = h\nu_{max}(abs) - h\nu_{max(f)} \cong \lambda_r + 2K_{exch} + 2(\epsilon_s - \epsilon_s') + \delta_{orb} + \delta_{vib} + \delta_{vib}' \qquad (22)$$

Since the reorganizational energies[80] and values of $2K_{exch}$[22,78,81] are expected to be of the order of a few thousands of wavenumbers, and since $H^2_{ge} < H^2_{eg}$, ϵ_s can also be expected to have values of the order of 2000 cm^{-1},[19,35,42] and the first three terms on the right side should dominate eq 22. However eqs21 and 22 need to be modified for the Cr(CN)Ru complexes.

While the exchange energy is probably a few thousand wavenumbers for the ^{3}MLCT excited state of $[Ru(NH_3)_4bpy]^{2+}$,[20,78,81] it is about 13000$-$14000 cm^{-1} (i.e., the energy difference between the ^{2}E and ^{4}A states) for the Cr(III) ground state. This implies that the sign of the K_{exch} contribution to $h\nu_{max(f)}$ must be positive for the Cr(CN)Ru systems (see eq 21). The $^4\{^4Cr^{III},Ru^{II}\}_g \rightarrow {}^4\{^3Cr^{II,2}Ru^{III}\}_{FC}$ absorption process will generate a low-spin (triplet) Cr^{II} species in a Franck$-$Condon MMCT excited state of quartet spin multiplicity. The emitting MMCT excited state must differ in spin multiplicity from the ground state, and it may contain either a low-spin $^3Cr^{II}$ center or a high-spin $^5Cr^{II}$ center; thus, the most likely electronic configurations for the long-lived, lowest energy MMCT excited states are $^2\{^3Cr^{II,2}Ru^{III}\}$ or $^6\{^5Cr^{II,2}Ru^{III}\}$. The highly distorted high-spin $^5Cr^{II}$ species is expected to have very large differences in metal$-$ligand bond lengths from those of the ground state,[21,82,83] and consequently very large amplitudes for their vibronic sideband contributions to the emission spectrum, and this does not seem to be the case for these complexes. Furthermore, the substantial stabilization of the (^{2}E)Cr^{III} excited state observed for the *trans*-[(*ms*-Me_6[14]aneN$_4$)Cr{CNRu$(NH_3)_5\}_2]^{5+}$ complex can only arise from configurational mixing with a ^{2}MMCT excited state. Thus, the $^2\{^3Cr^{II,2}Ru^{III}\}$ configuration seems most likely for the lowest energy MMCT excited state. The exchange energy of the $^2\{^3Cr^{II,2}Ru^{III}\}$ MMCT excited state is probably also large, but much smaller than that of the Cr(III) ground state. It is important to note that resonance Raman spectra indicate that there are very substantial distortions in the Ru$-$ligand vibrational modes even for the $[Ru(NH_3)_4bpy]^{2+}$ MLCT excited state,[65] and in this and in the $[(L)Cr\{CNRu(NH_3)_5\}_2]^{5+}$ complexes, the lowest frequency metal$-$ligand vibrational modes are convoluted into our estimate of the fundamental as a result of the large component bandwidths (i.e., all modes with $h\nu_l < {}^1/_2\Delta\nu_{1/2}$ will be convoluted into the fundamental),[35] so that λ_l could be larger for the MMCT than for the MLCT excited state. Finally, spin$-$orbit coupling is probably larger for H_{eg} in the ^{3}MLCT excited state than in the ^{2}MMCT excited state (as a result of the differences in separation of centers of spin density) so that one expects ϵ_s'(MLCT) $>$ ϵ_s'(MMCT) and the stabilization energy contribution ($\epsilon_s - \epsilon_s'$) to E_{ss} should be larger in the latter; this would partly compensate for the change of the sign of K_{exch}.

We have only considered the excited-state electronic configurations in this discussion. There are several electronic states that correspond to each of the MMCT excited-state configura-

tions and this could be relevant to interpreting the observations, but we have no information that relates to the more detailed assignment of these electronic excited states.

2. The Contrasting Effects of Configurational Mixing with LF Excited States. The lowest energy, triplet ligand field excited states of low-spin d^6 transition metal complexes involve population of an antibonding $d\sigma$ orbital and so they are typically very distorted.[84,85] Thus, the configurational mixing between such an excited state and a lower energy MLCT excited state is expected to result in greater distortion of the MLCT state along metal−ligand coordinates than would be the case for the diabatic limit. This is illustrated in Figure 1, and such configurational mixing seems to be supported by the relatively significant metal−ligand distortions found in the resonance Raman spectra of $[Ru(NH_3)_4bpy]^{2+}$ [65] and $[Ru(bpy)_3]^{2+}$ [67] and the apparent contributions of such modes to the 77 K emission spectra of these complexes.[23,39] In contrast, the (^{2}E)Cr(III) excited state has nearly the same nuclear coordinates as the ground state, so (^{2}E)Cr(III)/MMCT configurational mixing would have the effect of reducing the distortions in metal−ligand vibrational modes (see Figure 1). In the sense that increases in distortion tend to decrease excited-state lifetimes (all else being equal!), this effect might play a role in the observed contrasts on MMCT and MLCT excited-state lifetimes. However, the evaluation of any such effect requires consideration of multimode models for excited-state relaxation.

3. Possible Origins of the Contrasts between the Dependence of MMCT and MLCT Excited-State Lifetimes on the Dominant Distortion Modes. Figure 4 indicates that there are large qualitative differences in the parameters governing the nonradiative relaxation of the CT excited states of $[(L)_4Ru(bpy)]^{2+}$ and the $[(L')_4Cr(CNRu(NH_3)_5]^{n+}$ complexes. These differences are illustrated in the differences in the excited-state dynamics of the $[(NH_3)_4Ru(bpy)]^{2+}$ and the *trans*-[(MCL)Cr(CNRu$(NH_3)_5)_2]^{5+}$ complexes (MCL = [14]aneN$_4$ and *ms*-Me$_6$[14]aneN$_4$) that are the focus of this paper. Qualitatively, eq 16 implies that the smaller amplitudes and lower frequencies of the vibronic sideband contributions to the MMCT emissions than to the MLCT emissions should lead to longer lifetimes for the latter. However, the literal application of eq 16, a single mode limit and emrep parameters, implies that $k_{MMCT}/k_{MLCT} \sim 10^{-9}$, an 8 orders of magnitude greater difference than observed. This and the observations noted in the results section clearly demonstrate the limitations of eq 16 in treating multimode systems. Although there are notable discrepancies among the $[Ru(Am)_4bpy]^{2+}$ [38] complexes, as noted above, the biggest discrepancies appear to be for the MMCT decays, and these arise largely because the excited state is distorted in low-frequency vibrational modes (metal−ligand vibrational modes), and for such low-frequency modes eq 16 requires a prohibitively large number of vibrational quanta excited in the isoenergetic crossing from the MMCT excited states to the ground states. It is to be observed that effects of the contributions of low-frequency, metal−ligand distortion vibrational modes have been suggested as a source of these and the previously noted[38] deviations from simple correlations and that this suggestion has been made within the context of the models on which eq 16 is based, but in none of these instances has it been possible to evaluate the contributions of distortion modes with frequencies less than about 600 cm^{-1}. In the case of the [Ru([12]aneN$_4$)bpy]$^{2+}$ and [Ru([12]eneN$_4$]$^{2+}$ complexes, the longer MLCT excited-state lifetimes than those of related $[Ru(Am)_4bpy]^{2+}$ complexes are reasonably consistent with eq 16 and the inferred small values of $\Lambda_{x(max)}$(bpy). However, there is a possibility that unusually large low-frequency components are convoluted into the fundamental that we deconvoluted from the emission spectra of [Ru([12]aneN$_4$)bpy]$^{2+}$ and [Ru([12]eneN$_4$)bpy]$^{2+}$ and correction for this effect would result in significant discrepancies from correlations based on eq 16. This possibility is being further examined.[86]

In contrast to the general behavior observed for the $[Ru(Am)_4bpy]^{2+}$ complexes, the MMCT excited-state lifetimes are much shorter than those expected from eq 16 (due to the small value of $h\nu_{x(max)}$) for the *trans*-$[(MCL)Cr\{CNRu(NH_3)_5\}_2]^{5+}$ complexes. The very large isotope effects observed for the $[(MCL)Cr\{CNRu(NH_3)_5\}_2]^{5+}$ complexes indicate that the high-frequency N−H stretching modes are implicated in the relaxation process, but the resolution of such small (but significant) values of $\Lambda_{x(max)}$(NH) is only consistent with a much larger isotope effect; furthermore, $\Lambda_{x(max)}$(NH) is the upper limit for vibrational reorganizational energies of the high-frequency vibrational modes. Thus, eq 16 and the observed emrep parameters imply a value of $k_{NH}/k_{ND} \approx 3000$, while the observed values are only consistent with a substantially larger effective reorganizational energy ($\Lambda_{x(eff)}$(NH) $\sim$ 600 cm^{-1}; this would require $I_{max(f)}$(exptl) $\sim 20 I_{max(f)}$(actual)) of these high-frequency vibrational modes in a single mode model. Such a large distortion in the N−H modes is not consistent with the experimental emission spectra. Furthermore, the resolved values of $\Lambda_{x(max)}$(NH) $\sim$ 30 cm^{-1} with $h\nu_{x(max)}$ $\sim$3000 cm^{-1} would require a value of $A \sim 5 \times 10^{14}$ s^{-1} in the limit of a single distortion mode (eq 16) in order to account for the observed lifetimes. This obviously unreasonably large value of A arises because the distortions in the N−H stretching modes are so small. Since $\Lambda_{x(max)}$(NH) is a composite of the contributions of the 19 different N−H stretching modes in a localized (Cr^{II}(CN)-Ru^{III}) MMCT excited state, the actual distortion in any one of these modes must be even smaller and a single mode model, employing the actual distortion, would lead to an much larger value of A. One possible way to reconcile these observations with eq 16 is to consider the effect of multiple relaxation channels, each comprised of different combinations of distortion modes. For example, for N−H stretching modes only there could be 3000−4000 relaxation channels each involving a different combination of distortion modes and if each of these channels contributed a small amount to the excited-state relaxation, then a more realistic value of A would result. Furthermore, while the very large value of the isotope effects on the lifetimes of these complexes requires that the N−H stretching modes dominate the relaxation channels, they do not preclude some contributions from channels involving smaller contributions from the dominant distortion modes. Contributions from relaxation channels that include such lower frequency vibrational mode components would result in smaller isotope effects.

The delta function properties of the exponential factors in eqs 13 and 14 and relaxation channels with $h\nu_c = \sum_k n_k h\nu_k$ where $N_c = (n_1 + n_2 + n_3 + n_4 + ...)$ and $\nu'_c = \sum_k n_k h\nu_k \pm \lambda_s$ can be combined to represent the overall relaxation rate constant as

$$k_{et} \approx A \sum_c \left[\frac{1}{N_c!} \Pi_k \left(\frac{\lambda_k}{h\nu_k} \right)^{n_k} \right] \delta_{E^{0'0},\nu'_c} \qquad (23)$$

Equation 23 raises some very important issues in the accounting for the contributions of different relaxation channels: (a) By analogy with the contributions of combination as well as overtone frequencies to the bandshapes of emission spectra, we have defined a channel in terms of the sequence of the first-order vibrational contributions in eq 6 and there can be a very large number, d_c, of degenerate relaxation channels which differ only in the sequence of their first-order vibrational contributions. (b) The very strong excited state−ground state electronic coupling characteristic of Ru−bpy complexes[19,23,35] may require a different formalism. (c) Since the values of N_c involved are so large for all but the highest frequency vibrational modes, anharmonicities are likely to contribute.

Conclusions

The very weak vibronic contributions and therefore small distortions in high-frequency vibrational modes for the $[Ru(L)_4bpy]^{2+}$ and the $[(L')Cr\{CNRu(NH_3)_5\}]^{n+}$ complexes that has been found from analysis of the emission bandshapes can be compatible with the observed contrasts in excited-state lifetimes and isotope effects, while preserving the conceptual basis of common models for nonradiative relaxation and electron transfer if the overall rate constant is the sum of the contributions of a large number of excited-state distortion modes combined into a very large number of relaxation channels. Since we do not at present have a tractable multimode model, it is not possible to evaluate other factors that might contribute to these contrasts in excited state dynamics. For example, the metal−ligand distortions introduced into a MLCT excited state of Ru(II) by configurational mixing with a highly distorted ^{3}LF excited state might couple with the very large matrix elements for MLCT excited state Ru−bpy ground state configurational mixing to provide a uniquely efficient pathway for excited-state relaxation.

More generally, issues of excited-state−excited-state configurational mixing and multimode reaction channels are probably important in most inverted region ($|\Delta G^{o}_{eg}| > \lambda_s$) electron-transfer reactions.

Appendix

When the distortions, a_k, are small in the coordinates, Q_k, that correlate the differences in excited-state and ground-state geometries (i.e., $\lambda_k/h\nu_k \leq 0.1$, where $\lambda_k = {}^1/_2 f_k(a_k)^2$, then the intensity of the kth first-order vibronic contribution to the emission spectrum is given by[16,18]

$$I_{\max(k} = \left(\frac{\lambda_k}{h\nu_k}\right) I_{\max(f)} \tag{24}$$

Empirical reorganizational energy profiles (emreps) are based on eq 24 and generated by multiplying the difference spectrum by the difference between $h\nu_{\max(f)}$ and the observed emission energy ($h\nu_d = h[\nu_{\max(f)} - \nu_m]$). This generates an envelope of convoluted contributions of the reorganizational energies; thusthe first-, second-, and third-order contributions, respectively, to this envelope are given by ($w = \Delta\nu_{1/2}/(4 \ln 2)$)

$$\xi_i = h\nu_d \sum_i \left[\left(\frac{\lambda_i}{h\nu_i}\right) e^{-[G_i/w]^2}\right] \tag{25}$$

$$G_i = h\nu_{\max(f)} - h\nu_i$$

$$\xi_{ij} = h\nu_d \frac{1}{2} \sum_i \sum_j \left[\left(\frac{\lambda_i}{h\nu_i}\right)\left(\frac{\lambda_j}{h\nu_j}\right) e^{-[G_{ij}/w]^2}\right] \tag{26}$$

$$G_{ij} = h\nu_{\max(f)} - h\nu_i - h\nu_j$$

$$\xi_{ijk} = h\nu_d \frac{1}{6} \sum_i \sum_j \sum_k \left[\left(\frac{\lambda_i}{h\nu_i}\right)\left(\frac{\lambda_j}{h\nu_j}\right)\left(\frac{\lambda_k}{h\nu_k}\right) e^{-[G_{ijk}/w]^2}\right] \tag{27}$$

$$G_{ijk} = h\nu_{\max(f)} - h\nu_i - h\nu_j - h\nu_j$$

Since the functions described by eqs 25−27 are not Gaussian, a relatively simple correction has been made, based on the first-order vibronic terms, so that the maximum amplitudes of the individual reorganizational energy components occur at the frequencies corresponding to those of the distortion modes.[35] Thus for $h\nu_x = 2(h\nu_d) - [(h\nu_d)^2 + (\Delta\nu_{1/2})^2/(4 \ln 2)]^{1/2}$ and $\rho_i = \xi_i(\nu_x/\nu_d)$, etc.

$$\Lambda_x = \sum_i [\rho_i + \sum_j (\rho_{ij} + \sum_k \rho_{ijk})] \tag{28}$$

In summary: the emrep is obtained from the experimental spectrum by (a) determining a fundamental component by means of a careful fit of the observed spectrum using Grams 32, (b) subtracting the fundamental component from the observed spectrum (using data files in EXCEL) to obtain the difference spectrum, (c) constructing Λ_x based on eq 14, and then (d) plotting Λ_x vs $h\nu_x$[22,35,36] so that

$$\Lambda_x = h\nu_x\left(\frac{I_{\nu_m(diff)}}{I_{\max(f)}}\right) = \frac{h\nu_x}{I_{\max(f)}}(I_{\nu_m}(0'1) + I_{\nu_m(0'2)} + I_{\nu_m(0'3)} + ...) \tag{29}$$

This procedure provides information about the differences in reorganizational energy amplitudes for a closely related series of complexes; however, when there are a large number of vibrational modes whose energy differences ($\Delta h\nu_k$) are smaller than the component bandwidths ($\Delta\nu_{1/2}$) the emrep amplitudes will be much larger than any individual vibrational reorganizational energy, and if only first-order terms contribute in the frequency range of interest, then the emrep amplitude is less than or equal to the sum of all the first-order vibrational reorganizational energies. We have previously used the *rR* parameters for $[Ru(bpy)_3]^{2+}$ and $[Ru(NH_3)_4bpy]^{2+}$ to examine the implications and uncertainties of this procedure.[35] It is important to note that the procedures outlined here and presented in more detail elsewhere[35] are dependent on obtaining a good estimate of the fundamental and that the deconvolutions of the fundamental component have been shown to be reliable for Ru−bpy complexes when the fundamental is the dominant component of the spectrum (i.e., all $S_i \ll 1$) and for bandwidths less than about 1200 cm^{-1}.[35] The 77 K emission spectra of the complexes discussed here satisfy these conditions, and the estimates of $h\nu_{\max(f)}$ and $\Delta\nu_{1/2}$ deviate from of the correct values by much less than 10%.[35] In general, the *rR* modeling indicates

that the Grams32 fitting procedure does overestimate the intensity of the fundamental component for Ru−bpy complexes by 10−30% when $\Delta\nu_{1/2} \approx 1000$ cm^{-1} and the discrepancy increases with bandwidth as a consequence of the increasing overlap of the fundamental with low-frequency vibronic components.

Acknowledgment. It is a pleasure to acknowledge many years of challenging and stimulating interactions with Norman Sutin. The direct interactions have always been learning experiences and the potential for Norman's critical comments is an ever-present discipline on the written word. The authors thank the Office of Basic Energy Sciences of the Department of Energy for partial support of this research.

Supporting Information Available: Figures showing the difference between the absorption spectrum of *trans*-[(*ms*-Me_6-[14]aneN$_4$)Cr{CNRu(NH$_3$)$_5$}$_2$]$^{5+}$ and a Gaussian fitting function, emission spectra of [Cr([15]aneN$_4$)(CN)$_2$]$^+$ and [Cr([15]aneN$_4$)-(CNHg)$_2$]$^{5+}$, comparison of the fits of a single distortion mode to the difference spectra of [Ru(bpy)$_3$]$^{2+}$ and [Ru(NH$_3$)$_4$bpy]$^{2+}$, one and two "equivalent" distortion mode fits of the difference spectrum of [Ru(bpy)$_3$]$^{2+}$, qualitative PE curves illustrating the effects of configurational mixing between a (^{2}E)Cr^{III} excited-state and two degenerate MMCT excited states and comparison of the 77 K MMCT and MLCT emission spectra and Table S1 showing the parameters for two component fits of MMCT excited-state decay. This material is available free of charge via the Internet at http://pubs.acs.org.

References and Notes

(1) Marcus, R. A. *Discuss. Faraday Soc.* **1960**, *29*, 21.
(2) Sutin, N. *Annu. Rev. Nucl. Sci.* **1962**, *12*, 285.
(3) Marcus, R. A. *Annu. Rev. Phys. Chem.* **1964**, *15*, 155.
(4) Hush, N. S. *Prog. Inorg. Chem.* **1967**, *8*, 391.
(5) Sutin, N. *Acc. Chem. Res.* **1982**, *15*, 275.
(6) Sutin, N. *Prog. Inorg. Chem.* **1983**, *30*, 441.
(7) Newton, M. D.; Sutin, N. *Annu. Rev. Phys. Chem.* **1984**, *35*, 437.
(8) Englman, R.; Jortner, J. *Mol. Phys.* **1970**, *18*, 145.
(9) Freed, K. F.; Jortner, J. *J. Chem. Phys.* **1970**, *52*, 6272.
(10) Kestner, N.; Logan, J.; Jortner, J. *J. Phys. Chem.* **1974**, *64*, 2148.
(11) Sutin, N.; Brunschwig, B. S. In *Electron Transfer in Biology and the Solid State*; Advances in Chemistry Series 226; American Chemical Society: Washington, DC, 1990; p 64.
(12) Sutin, N. *Adv. Chem. Phys.* **1999**, *106*, 7.
(13) Brunschwig, B. S.; Sutin, N. In *Electron Transfer in Chemistry*; Balzani, V., Ed.; Wiley-VCH: Weinheim, 2001; Vol. 2; pp 583.
(14) *Electron Transfer in Chemistry*; Balzani, V., Ed.; Wiley-VCH: Weinheim, Germany, 2001; Vol. 1−5.
(15) Steinfeld, J. I. *Molecules and Radiation, an Introduction to Modern Molecular Spectroscopy*; MIT Press: Cambridge, MA, 1981.
(16) Solomon, E. I. *Comments Inorg. Chem.* **1984**, *3*, 225.
(17) Gould, I. R.; Noukakis, D.; Gomez-Jahn, L.; Young, R. H.; Goodman, J. L.; Farid, S. *Chem. Phys.* **1993**, *176*, 439.
(18) Brunold, T. C.; Gudel, H. U. In *Inorganic Electronic Structure and Spectroscopy*; Solomon, E. I., Lever, A. B. P., Eds.; Wiley-Interscience: New York, 1999; Vol. 1; pp 259.
(19) Seneviratne, D. S.; Uddin, M. J.; Swayambunathan, V.; Schlegel, H. B.; Endicott, J. F. *Inorg. Chem.* **2002**, *41*, 1502.
(20) Endicott, J. F.; Schegel, H. B.; Uddin, M. J.; Seneviratne, D. *Coord. Chem. Rev.* **2002**, *229*, 95.
(21) Endicott, J. F. In *Comprehensive Coordination Chemistry II*, 2 ed.; McCleverty, J., Meyer, T. J., Eds.; Pergamon: Oxford, U.K., 2003; Vol. 7; p 657.
(22) Endicott, J. F.; Chen, Y.-J.; Xie, P. *Coord. Chem. Rev.* **2005**, *249*, 343.
(23) Endicott, J. F.; Chen, Y.-J. *Coord. Chem. Rev.* **2007**, *251*, 328.
(24) Meyer, G. J. *Inorg. Chem.* **2005**, *44*, 6852.
(25) Dempsey, J. L.; Esswein, A. J.; Manke, D. R.; Soper, J. D.; Nocera, D. G. *Inorg. Chem.* **2005**, *44*, 6879.
(26) Chakraborty, S.; Wadas, T. J.; Hester, H.; Schmehl, R. H.; Eisenberg, R. *Inorg. Chem.* **2005**, *44*, 6865.
(27) Alstrum-Acevedo, J. H.; Brennaman, M. K.; Meyer, T. J. *Inorg. Chem.* **2005**, *44*, 6802.
(28) Hoertz, P., G.; Mallouk, T. E. *Inorg. Chem.* **2005**, *44*, 6828.
(29) Marcus, R. A. *J. Phys. Chem.* **1990**, *94*, 4963.
(30) Marcus, R. A.; Sutin, N. *Biochim. Biophys. Acta* **1985**, *811*, 265.
(31) Piotrowiak, P. *Chem. Soc. Rev.* **1999**, *28*, 143.
(32) Barbara, P. F.; Meyer, T. J.; Ratner, M. *J. Phys. Chem.* **1996**, *100*, 13148.
(33) Bolvin, H. *Inorg. Chem.* **2007**, *46*, 417.
(34) Lever, A. B. P. *Inorganic Electronic Spectroscopy*; Elsevier: Amsterdam, 1984.
(35) Xie, P.; Chen, Y.-J.; Uddin, M. J.; Endicott, J. F. *J. Phys. Chem. A* **2005**, *109*, 4671.
(36) Chen, Y.-J.; Xie, P.; Endicott, J. F. *J. Phys. Chem. A* **2004**, *108*, 5041.
(37) Chen, Y.-J.; Xie, P.; Endicott, J. F.; Odongo, O. S. *J. Phys. Chem. A* **2006**, *110*, 7970.
(38) Chen, Y.-J.; Xie, P.; Heeg, M. J.; Endicott, J. F. *Inorg. Chem.* **2006**, *45*, 6282.
(39) Xie, P.; Chen, Y.-J.; Endicott, J. F.; Uddin, M. J.; Seneviratne, D.; McNamara, P. G. *Inorg. Chem.* **2003**, *42*, 5040.
(40) Endicott, J. F.; McNamara, P. G.; Buranda, T.; Macatangay, A. V. *Coord. Chem. Rev.* **2000**, *208*, 61.
(41) Watzky, M. A.; Endicott, J. F.; Song, X.; Lei, Y.; Macatangay, A. V. *Inorg. Chem.* **1996**, *35*, 3463.
(42) Watzky, M. A.; Macatangay, A. V.; Van Camp, R. A.; Mazzetto, S. E.; Song, X.; Endicott, J. F.; Buranda, T. *J. Phys. Chem.* **1997**, *101*, 8441.
(43) Hay, R. W.; Lawrence, G. A.; Curtis, N. F. *J. Chem. Soc., Perkin Trans.* **1975**, 591.
(44) Barefied, E. K.; Wagner, F.; Herlinger, A. W.; Dahl, A. R. *Inorg. Synth.* **1976**, *16*, 221.
(45) Habib, H. S.; Hunt, J. P. *J. Am. Chem. Soc.* **1966**, *88*, 1668.
(46) Hung, Y. *Inorg. Synth.* **1980**, *20*, 108.
(47) Barefied, E. K.; Wagner, F. *Inorg. Synth.* **1976**, *16*, 220.
(48) Barefied, E. K.; Freeman, G. *Inorg. Synth.* **1980**, *20*, 108.
(49) Herve, G.; Bernard, B.; Le Bris, N.; Yaouanc, J.-J.; Handel, H.; Toupet, L. *Tetrahedron Lett.* **1998**, *39*, 6861.
(50) Karn, J. L.; Busch, D. H. *Inorg. Chem.* **1969**, *8*, 1149.
(51) Krentzien, H. J. Ph.D. Dissertation, Stanford University, 1976.
(52) Kane-Maguire, N. A. P.; Cripeen, W. S.; Miller, P. K. *Inorg. Chem.* **1983**, *22*, 696.
(53) Lessard, R. B.; Heeg, M. J.; Buranda, T.; Perkovic, M. W.; Schwarz, C. L.; Rudong, Y.; Endicott, J. F. *Inorg. Chem.* **1992**, *31*, 3091.
(54) Krause, R. A. *Inorg. Chim. Acta* **1977**, *22*, 209.
(55) Evans, I. P.; Spencer, A.; Wilkinson, G. *J. Chem. Soc., Dalton Trans.* **1973**, 204.
(56) Curtis, J. C.; Sullivan, B. P.; Meyer, T. J. *Inorg. Chem.* **1983**, *22*, 224.
(57) Song, X.; Lei, Y.; Van Wallendel, S.; Perkovic, M. W.; Jackman, D. C.; Endicott, J. F.; Rillema, D. P. *J. Phys. Chem.* **1993**, *97*, 3225.
(58) Myers, A. B. *Chem. Rev.* **1996**, *96*, 911.
(59) Myers, A. B. *Acc. Chem. Res.* **1998**, *30*, 519.
(60) Myers, A. B. In *Laser Techniques in Chemistry*; Myers, A. B., Rizzo, T. R., Eds.; John Wiley & Sons, Inc., 1995; Vol. XXIII; p 325.
(61) Yardley, J. T. *Introduction to Molecular Energy Transfer*; Academic: New York, 1980.
(62) Crosby, G. A.; Elfring, W. N., Jr. *J. Phys. Chem.* **1978**, *80*, 2206.
(63) Macatangay, A. V.; Endicott, J. F. *Inorg. Chem.* **2000**, *39*, 437.
(64) Supporting information. See the paragraph at the end of this paper.
(65) Hupp, J. T.; Williams, R. T. *Acc. Chem. Res.* **2001**, *34*, 808.
(66) Ryu, C. K.; Lessard, R. B.; Lynch, D.; Endicott, J. F. *J. Phys. Chem.* **1989**, *93*, 1752.
(67) Maruszewski, K.; Bajdor, K.; Strommen, D. P.; Kincaid, J. R. *J. Phys. Chem.* **1995**, *99*, 6286.
(68) Chernyak, V.; Mukamel, S. *J. Chem. Phys.* **1996**, *105*, 4565.
(69) Meyer, T. J. *Prog. Inorg. Chem.* **1983**, *30*, 389.
(70) Kober, E. M.; Casper, J. V.; Lumpkin, R. S.; Meyer, T. J. *J. Phys. Chem.* **1986**, *90*, 3722.
(71) Graff, D.; Claude, J. P.; Meyer, T. J. In *Electron Transfer Reactions: Inorganic, Organometallic and Biological Applications*; Isied, S. S., Ed.; American Chemical Society: Washington, DC, 1997; p 183.
(72) Thompson, D. G.; Schoonover, J. R.; Timpson, C. J.; Meyer, T. J. *J. Phys. Chem. A* **2003**, *107*, 10250.
(73) Casper, J. V.; Kober, E. M.; Sullivan, B. P.; Meyer, T. J. *J. Am. Chem. Soc.* **1982**, *104*, 630.
(74) Chen, Y.-J.; Endicott, J. F.; Swayambunathan, V. *Chem. Phys.* **2006**, *326*, 79.
(75) Ryu, C. K.; Endicott, J. F. *Inorg. Chem.* **1988**, *27*, 2203.
(76) Matyushov, D. V.; Voth, G. A. *J. Phys. Chem. A* **2000**, *104*, 6470.

(77) Matyushov, D. V.; Newton, M. D. *J. Phys. Chem. A* **2001**, *105*, 8516.
(78) Endicott, J. F.; Uddin, M. J.; Schlegel, H. B. *Res. Chem. Intermed.* **2002**, *28*, 761.
(79) Macatangay, A. V.; Song, X.; Endicott, J. F. *J. Phys. Chem.* **1998**, *102*, 7537.
(80) Endicott, J. F. In *Electron Transfer in Chemistry*; Balzani, V., Ed.; Wiley-VCH: New York, 2001; Vol. 1; p 238.
(81) Lever, A. B. P.; Gorelsky, S. I. *Coord. Chem. Rev.* **2000**, *208*, 153.
(82) Meyer, T. J.; Taube, H. In *Comprehensive Coordination Chemistry*; Wilkinson, G., Gillard, R. D., McCleverty, J., Eds.; Pergamon: Oxford, England, 1987; Vol. 7; p 331.
(83) Endicott, J. F.; Kumar, K.; Ramasami, T.; Rotzinger, F. P. *Prog. Inorg. Chem.* **1983**, *30*, 141.
(84) Wilson, R. B.; Solomon, E. I. *J. Am. Chem. Soc.* **1980**, *102*, 4085.
(85) Hakamata, K.; Urushiyama, A.; Kupka, H. *J. Phys. Chem.* **1981**, *85*, 1983.
(86) Odongo, O. S.; Chen, Y.-J.; Endicott, J. F. Work in progress.